

## Thermal method to determine crack nucleation conditions under fretting loading

by B. Berthel\* and S. Fouvry\*

\*LTDS, Ecole Centrale de Lyon, 36, Avenue Guy de Collongue, Ecully 69134 Cedex, France, [bruno.berthel@ec-lyon.fr](mailto:bruno.berthel@ec-lyon.fr)

### Abstract

The aim of this study is to develop a new experimental method to measure temperature field during a fretting test in a cylinder on flat contact configuration. Analyze of temperature evolution during a fretting test with constant loading shows that this latter can be decompose on a global warming and a sum on two periodic signal at  $f_L$  and  $2f_L$ , where  $f_L$  is the loading frequency. Analyze of the global warming during a fretting test with step by step increasing of tangential force unable us to develop an empirical method to determine the crack nucleation conditions.

### 1. Introduction

Fretting loadings cause damages which decrease highly the lifetime of industrial systems This phenomenon is characterized by very small sliding amplitudes significantly smaller than the contact size, which may occur between contacting surfaces that are subjected to vibration or cyclic stress. All industrial domains are concerned: transport, energy,... [1]. Fretting damage on the contacting surface is critically controlled, under sliding conditions, by the amplitude of slip displacement [2][3]. Under large amplitude gross slip conditions, where the whole surface is fretted and wear processes associated with debris formation and ejection dominate, friction energy wear models have been introduced [4]. Under partial slip conditions, initiation of fatigue cracks is generally a more significant concern than wear. This micro-slip can give rise to embryo cracks very early in life.

Determination of crack nucleation conditions requires time-consuming and expensive destructive methods giving dispersive results [5]. Analyses consist of an optical determination of the crack length. For all fretting tests, the sample is cut in the middle of the scars. Then, the new surface created is polished and observed with an optical microscope (cf. §2.3).

Several approaches consider fretting loading under stabilized partial slip condition like mutiaxial fatigue loaging with stress gradient and It has been shown that crack nucleation can be predicted by transposing multiaxial fatigue criteria (Dang Van, Crossland,...) [6][7][8]. Like in fatigue, cracks initiation is directly linked to the plastic response of the material at the micro-scale. The local microscopic stress can locally exceed the yield strength in certain unfavorably oriented grains, whereas the macroscopic stress remains elastic. If the cyclic plastic response of the grain is not an elastic shakedown, then some microcracks will be nucleated.

Assuming that the temperature of a specimen during a fatigue test is an indicator of plastic at the microscopic scale, alternative thermal methods based on an analysis of self-heating during a stepwise loading fatigue test have been developed to rapidly provide reliable fatigue characteristics [9][10][11][12][13]. The authors of these latter studies claimed that the remarkable change in the heating regime, observed at a certain stress range, is empirically related to the fatigue limit of the material. These methods were extended to multiaxial fatigue test [14]. In [15] it was shown that the appearance of the persistent slip bands is associated with the loss of linearity of the temperature vs. stress range correspondence. It was also shown that the persistent slip band number increases with the stress and appears to be a relevant fatigue indicator. During a fatigue test on thin flat steel specimen, in [16] it was observed a localisation of the plastic phenomenon on the dissipative field (obtained by an inverse method) until the beginning of the test and the area corresponding to the crack onset is also found to be an area where dissipation was high. This result shows that plasticity observed at a mesoscopic scale and crack nucleation are linked.

The aim of this study is to transpose these thermal methods to the fretting loading to determine crack nucleation conditions. From a mechanical point of view, the plastic behaviour of material under cyclic loadings which drive the crack nucleation in fatigue and fretting are the same: elastic shakedown, plastic shakedown and ratcheting phenomena.

This work is performed in the framework of FAST3D research project (Coupling between direct cyclic methods in structural computation and dissipative full-field measurements: a strategy for a fast determination of crack initiation map in fretting-fatigue) financed by the French National Research Agency (ANR). In this paper, the very first results of this work were shown.

### 2. Experimental conditions and conventional method

#### 2.1. Material and contact parameters

Cylinder on flat configuration was chosen for this study. The material used for fretting sample is a steel alloy 35NCD16 with a specified heat treatment. Pads is made of heat treated steel 100 C6 with a controlled roughness ( $R_a =$

0.4µm). The mechanical properties are shown in Table 1. The cylinder radius is  $R = 80$  mm, the pad and the flat lengths are  $L = 8$  mm, giving plane strain conditions near the central axis of the fretting scar.

**Table 1.** Mechanical characteristic of steel alloys

	E (GPa)	$\nu$	$\sigma_y$ (MPa)	$\sigma_u$ (MPa)
35NCD16	199	0,29	1200	1430
100C6	194		1500	-

**2.2. Fretting experimental set-up**

This experimental set-up is based on a fretting device mounted to a servo hydraulic test machine (cf. Fig. 1). Further details of this set-up and the experimental methods can be found in [17]. Once the specimen is fixed and carefully aligned with the counter body, a constant normal force  $P$  is applied followed by a cyclic sinusoidal displacement  $\delta$  at a frequency  $f_L$  in order to generate an alternative cycle tangential load  $Q$  on the contact surface, perpendicular to the sliding direction. During the tests  $P$ ,  $Q$  and  $d$  are continuously recorded.  $Q^*$  and  $\delta^*$  denote their amplitudes. Fretting tests performed to determine crack nucleation are all performed at  $10^6$  cycles and  $f_L = 10$  Hz. Four maximal Hertzian pressures  $p_{max}$ , giving rise to four normal loads  $P$  (cf. Table2), were tested: 460MPa, 670MPa, 800MPa and 1000MPa.

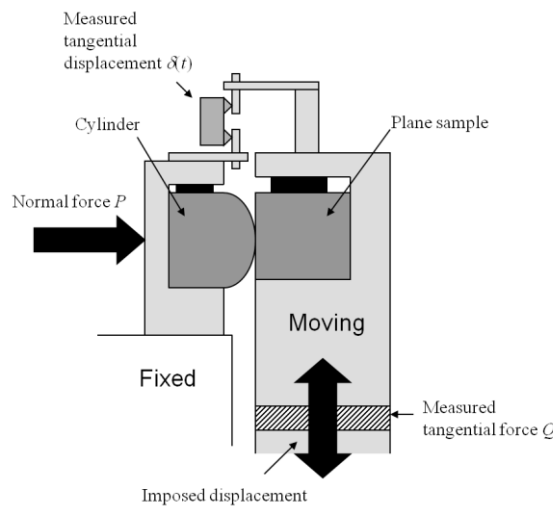


**Fig. 1.** Schematic diagram of the fretting device [18]

**2.3. Destructive experimental procedure**

Previous tests were performed to determine crack nucleation threshold by conventional method and this latter is describe in this part. For each normal load  $P$ , several tangential load amplitudes  $Q^*$  are tested to locate the crack initiation threshold. All of the tests are investigated with respect to the following methodology. Analyses consist of a determination of the crack depth through cross section observation. This crack analysis technique has been inspired by Proudhon *et al.* [19]. For all fretting tests, an optical micrograph of the fretting scar is recorded after the test. The sample is then cut in the middle of the scar perpendicular to the fretting loading. Then, the new surface created is polished and observed with an optical microscope (cf. Fig. 2). The crack length and crack depth are measured. Note that the polishing and observation phase is repeated triple in order to evaluate the homogeneity of the crack data. Only maximal cracks lengths were considered.

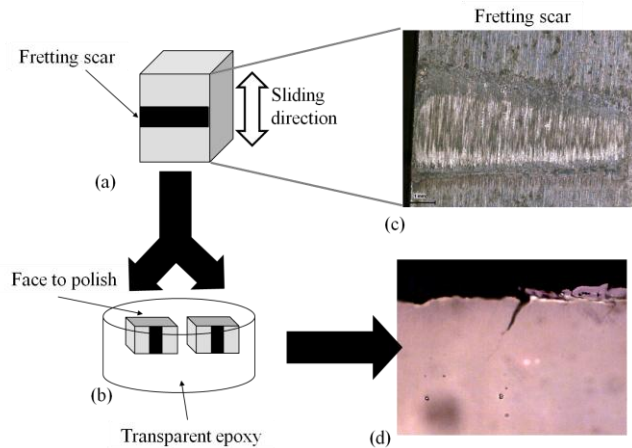


**Fig. 2.** Experimental method to investigate cracking after fretting test; see the text for details.

Therefore a threshold regarding the crack depth is defined to consider if crack initiated or not. This threshold is set at 10 μm. This threshold is supposed to be low enough to get the incipient crack initiation and large enough to claim that a crack initiated. This methodology to determine the crack nucleation threshold is presented in Fig. 3. Results obtained by this method are presented in Table 2. This method is very time consuming and expensive in term of material. About one month in full-time was necessary to obtain the results in Table 2 and twenty specimens.

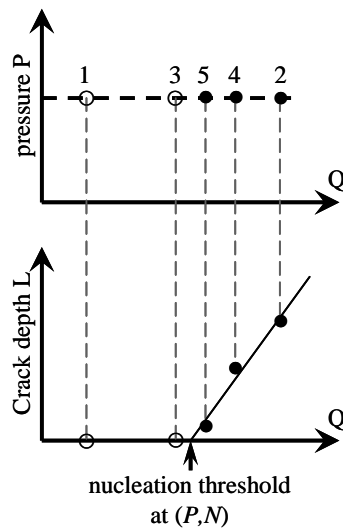


**Fig. 3.** Methodology used to determine the crack nucleation threshold

**Table 2.** tangential amplitude  $Q^*$  given rise to a fretting crack estimate by destructive method  $Q_D$

$P_{max}$ (MPa)	$P/L$ (N/mm)	$Q_D/L$ (N/mm)
460	469	242
670	994	333
800	1413	399
1000	2208	470

Previously, the coefficient of friction in partial slip regime of the material couple was measured using the variable amplitude method. Details about this method are available in [19]. The coefficient of friction  $\mu$  was found equal to 0.8.

### 3. Thermal method

#### 3.1. Thermal measurement

The camera used in this work is a FLIR SC7600 MWIR 2.5-5 $\mu$ m. The focal length of the optical lens is 25 mm. This camera is equipped with an InSb 640x512 element detector. The maximal frame rate  $f_a$  is 380Hz and the noise-equivalent temperature (NET) is lower than 25mK. In this study the size of a pixel is about 0.16x0.16 mm<sup>2</sup>. The lens axis of the camera was kept fixed and held perpendicular to the lateral surface of the specimen during the mechanical tests (cf. Fig. 4). Steel alloys have a high conductivity factor, so it is assuming that the thermal image is very close to the temperature below the contact. Flat specimen and cylinder lateral surfaces are coating with a black matt paint to increase its emissivity.

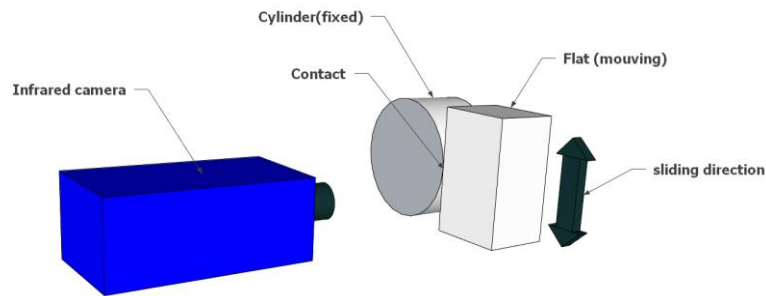


Fig. 4. Schematic diagram of the camera position

For this first test in this project, a macroscopic scale was chosen. At this scale, specimen deformations can be neglected. Temperature is average over a Zone Of Interest (ZOI - cf. Fig. 5). The size of this zone is characterized the Hertzian contact size  $a$ .

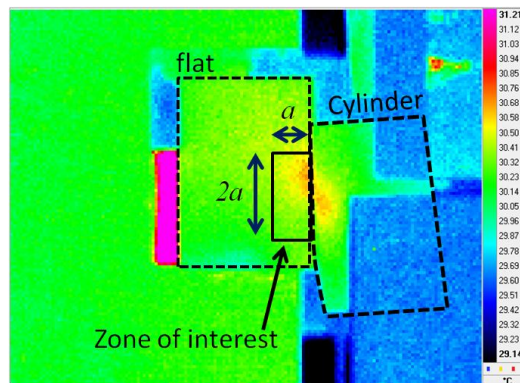


Fig. 5. temperature field during a fretting test

#### 3.2. Rigid body movement correction

Vibrations and flexibility of the experimental device impose rigid movement body on the flat specimen. Center of the contact is stuck, thus without these phenomenon displacements must be very low. Rigid movement body must be determining and corrected on temperature fields to follow the ZOI on the specimen. A markers tracking method based on edge detection, basic morphology, filtering and thresholding tools to determine the center of mass of regions was chosen. Different type and localisations of markers were tested. In this paper, marker was made by emissivity contrast (unpainted circles in a painted region) and localised on a patch fixed on the moving arm of the fretting device (cf. Fig 6)

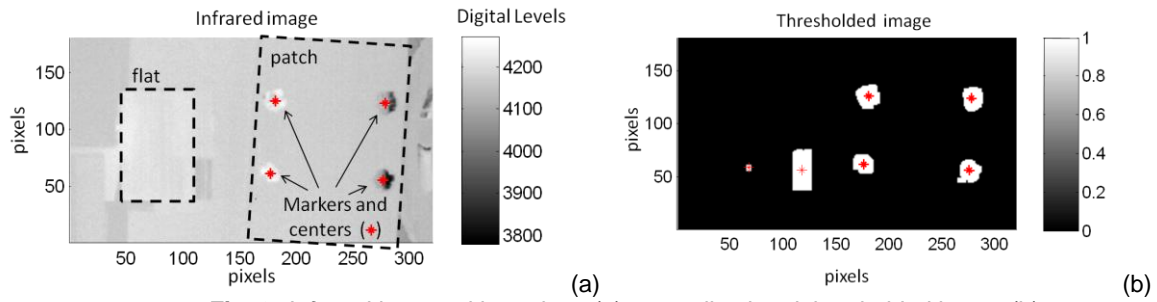


Fig. 6. Infrared image with markers (a); normalized and thresholded image (b)

Successive positions of the markers in the infrared film allow us to determine the rigid transformation (rotation and translation) by a least square method between the first image and all other images. The ZOI is chosen on the first image and the transformation is applied on this latter in all other.

### 3.3. Temperature evolution during a fretting test at constant loading

Temperature evolutions on a pixel near the contact and averaged over the ZOI during a fretting test with  $P/L=1000\text{N/mm}$ ,  $Q/L=600\text{N/mm}$ ,  $f_L=5\text{Hz}$  and  $f_a=50\text{Hz}$  are shown in Fig 7. On these latter, it can be observed a global warming of about  $0.5^\circ\text{C}$ , superimposed to oscillatory variation of temperature with maximal amplitude of about  $0.05^\circ\text{C}$ . Temperature stabilization is reached after several numbers of cycles.

To identify frequency components of these thermal signals, discrete Fourier transformations are performed on the oscillatory part of the temperature evolution and amplitude spectrums are shown in Fig 8. In the two cases, a high level amplitude and a lower amplitude level can be observed respectively at  $f_L$  and  $2 f_L$ . We can assume that the high amplitude at  $f_L$  is induced by thermoelastic effect then amplitude at  $2 f_L$  and the global warming are induced by several dissipative effects like plasticity and friction in the sliding zone of the contact.

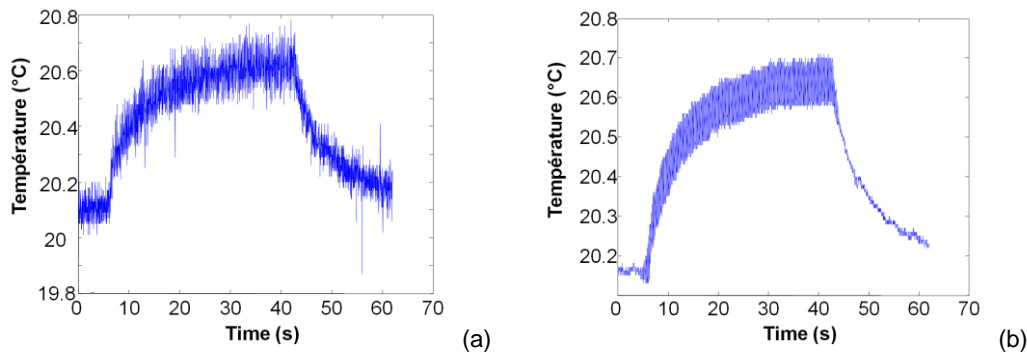


Fig. 7. Temperature evolution on a pixel (a) and averaged over the ZOI (b) during a fretting test with

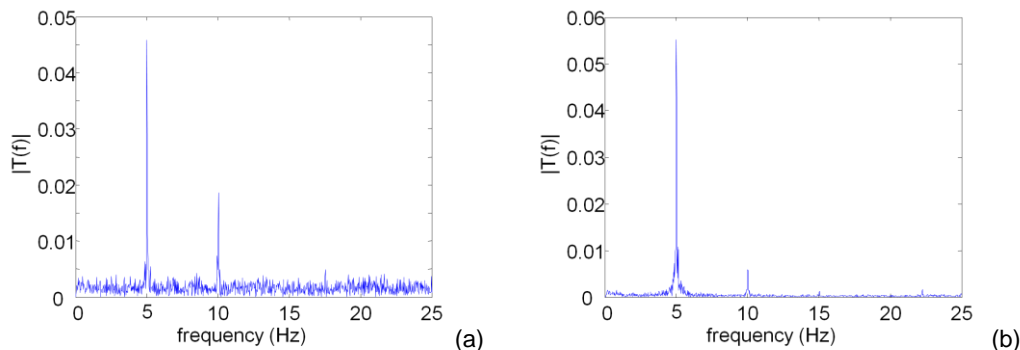


Fig. 8. Single-sided amplitude spectrum of the oscillatory part of the temperature on a pixel (a) and averaged over the ZOI (b)

Among several possible methods, a local least-squares fitting of the thermal signal was considered in this work like in [16] and [20]. The temperature approximation functions account for the spectral properties underlying previously. The local fitting function  $T^{\text{fit}}$  of the temperature charts is chosen like this:

$$T^{\text{fit}}(x, y, \tau) = \underbrace{p_1 + p_2 t}_{\text{linear drift}} + \underbrace{p_3 \cos(2\pi f_L \tau) + p_4 \sin(2\pi f_L \tau)}_{\text{periodic signal at } f_L} + \underbrace{p_5 \cos(4\pi f_L \tau) + p_6 \sin(4\pi f_L \tau)}_{\text{periodic signal at } 2f_L} \quad (1)$$

where the trigonometric time functions at  $f_L$  describe the periodic part of the thermoelastic effects while the linear time function and the periodic part at  $2f_L$  takes transient effects due to heat losses, dissipative heating and possible drifts in the equilibrium temperature into account. The same form of the fitting function was applied to the temperature variation  $\theta = T - T_0$ , where  $T_0$  is the equilibrium temperature at the beginning of the test. The difference between approximate temperature and experimental temperature on a pixel and averaged over the ZOI are shown in Fig. 8. The mean value and standard deviation of these latter are respectively  $32 \cdot 10^{-3} \text{ }^\circ\text{C}$  and  $25 \cdot 10^{-3}$  for the pixel evolution,  $8 \cdot 10^{-3} \text{ }^\circ\text{C}$  and  $7 \cdot 10^{-3}$  for the ZOI evolution. The difference is higher in the case of the temperature on a pixel. It is the consequence of noisier data but this latter is in the same order of magnitude of the NET of the camera. In Fig 8(b), we can observe two local maximum corresponding to the beginning and the end of the cyclic loading.

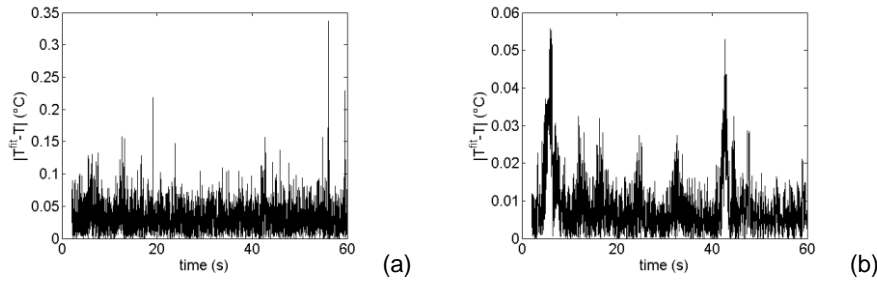


Fig. 8. Differences between the temperature of a pixel (a), the averaged temperature on the ZOI (b) and the fitted function.

Amplitudes of periodic signals at  $f_L$  and  $2f_L$ , respectively  $A_f$  and  $A_{2f}$ , can be define by:

$$A_f = \sqrt{p_3^2 + p_4^2} \quad (2)$$

$$A_{2f} = \sqrt{p_5^2 + p_6^2} \quad (3)$$

Fig 9 and Fig 10 show evolutions of global warming,  $A_f$  and  $A_{2f}$ . In the two cases,  $A_f$  remains constant during the test as expected, if this latter is considered as an indicator of the thermoelastic effect.  $A_{2f}$  is noisier  $A_f$  than but in first approximation we can assume that is also constant.

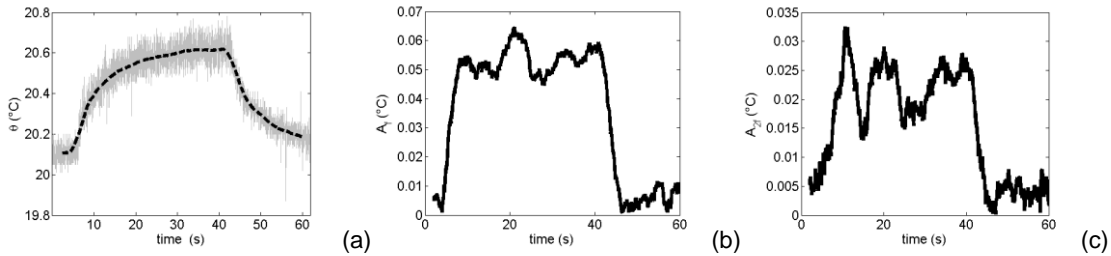


Fig. 9. Results of temperature evolution on a pixel fitting: (a) linear drift, (b)  $A_f$  and (c)  $A_{2f}$ .

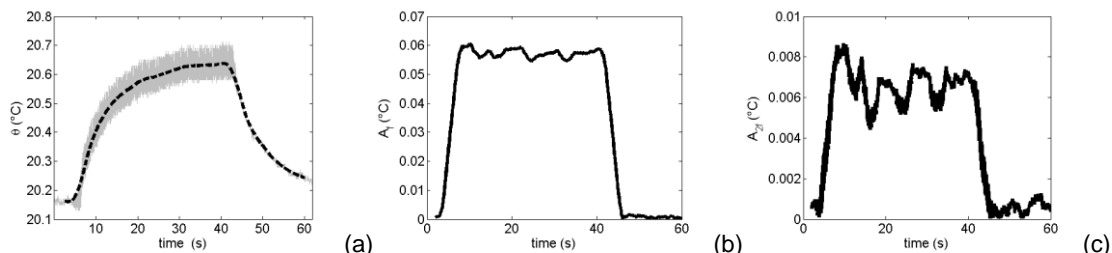


Fig. 10. Results of temperature evolution on a pixel fitting: (a) linear drift, (b)  $A_f$  and (c)  $A_{2f}$ .

### 3.4. Temperature evolution during a fretting test at P constant

For each  $p_{max}$  variable displacement tests (cf. §2.2) were made [19]: the normal load is kept constant whereas the relative displacement amplitude ( $\delta^*$ ) starts from a very low value, imposing a clear partial slip condition (with  $Q^* < \mu P$ , where  $\mu$  is the coefficient of friction). When stabilized mechanical and thermal conditions are reached,  $\delta^*$  is increased and then maintained constant until a new stable situation is reached. The imposed displacement,  $\delta^*$ , is increased in this way, step by step, until the contact makes the transition to sliding ( $Q^* = \mu P$ ) (cf. Fig 11(a)). During each step, evolution of the temperature field on the surface of the flat is record by the infrared camera. The variation of average temperature over the ZOI  $\theta = T - T_0$ , where  $T_0$  is the equilibrium temperature at the beginning of the test, is plot in Fig11(b) for  $p_{max} = 670\text{MPa}$ . At each step, the variation of temperature reach a stabilized value  $\theta_{sta}$ . High acquisition frequency with the infrared camera can't be used because tests durations are very long. A frequency  $f_a = 11\text{Hz}$  was chosen to determine only  $\theta_{sta}$  at each step. To determine this latter the fitting method developed previously was used. Evolutions of  $A_f$  and  $A_{2f}$  as in [13] will be studied in futures works.

At the beginning of each step, a small number of cycles in gross slip can be induced by instability of the contact or the hydraulic actuator response. These latter introduce short but high increase of the variation of temperature that can be observed in Fig 11(b).

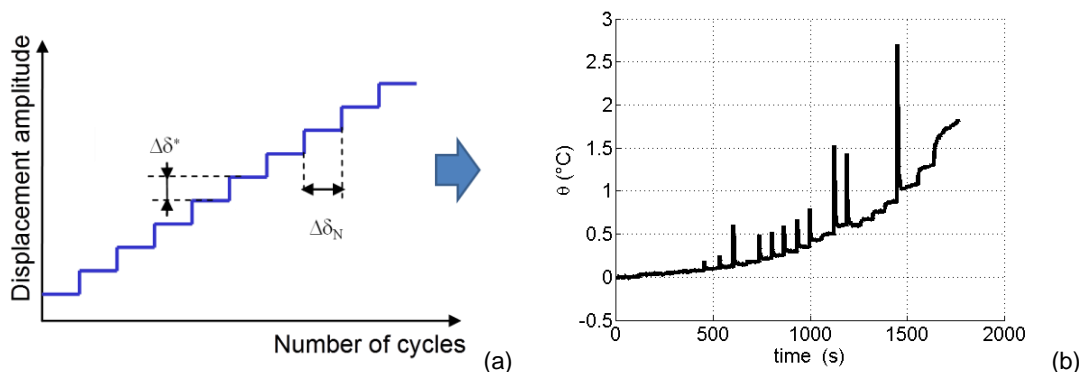
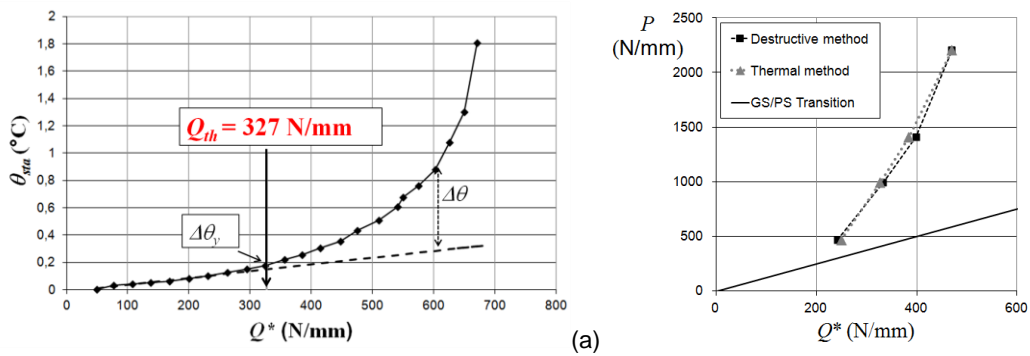


Fig. 11. (a) Principle of a variable displacement test ;(b) evolution of the variation of temperature during a variable displacement test for  $p_{max} = 660\text{MPa}$

The evolution of  $\theta_{sta}$  can be considered as an indicator of the microplastic behavior of the material and then an indicator of the crack initiation. The slope change in evolution of the stabilized value  $\theta_{sta}$  of all step vs. the tangential amplitude  $Q^*$  in Fig. 12(a) can be empirically connected with the critical tangential amplitude  $Q_{th}$  giving rise to a fretting crack by the method describe in the next paragraph.

For each  $p_{max}$ , a linear regression of  $\theta_{sta}(Q^*)$  for  $Q^* < 0.4P$  was made to determine the difference  $\Delta\theta$  between this linear regression and  $\theta_{sta}$  for all  $Q^*$  (cf. Fig. 12(a)). To adjust the method, at  $p_{max} = 1000\text{MPa}$  a yield value  $\Delta\theta_y$  of  $\Delta\theta$  was chosen corresponding to  $\Delta\theta$  at the crack threshold  $Q_D$  obtained by the destructive method. Linear approximation of  $\theta_{sta}(Q^*)$  was used to determine  $\Delta\theta$  between two experimental values of  $Q^*$ . In these tests,  $\Delta\theta_y$  was set equal to  $31 \cdot 10^{-3} \text{ } ^\circ\text{C}$ . Finally, for all other  $p_{max}$ ,  $Q^*$  corresponding to  $\Delta\theta_y$  is chosen as the crack threshold  $Q_{th}$  obtained by the thermal method (cf. exemple Fig. 12(a)). Fig. 12(b) show the comparison between results obtained with destructive method resulting of severals days of expertise and thermal method developed in this paper for four levels of  $P$ . Table 3. show numerical values of these thresholds. Last colum of Table 3 show error define by  $|Q_D - Q_{th}|/Q_D$ . This erros remains inferior to 4% for all tests.



**Fig. 12.** (a) Evolution of  $\theta_{sta}$  vs.  $Q^*$  (b) Comparisons between tangential amplitude  $Q^*$  ginvin rise to a fretting crack estimate by destructive method  $Q_D$  and thermal method  $Q_{th}$

**Table 3.** Comparisons between tangential amplitude  $Q^*$  ginvin rise to a fretting crack estimate by destructive method  $Q_D$  and thermal method  $Q_{th}$

$p_{max}$ (MPa)	$P/L$ (N/mm)	$Q_{th}/L$ (N/mm)	$Q_D/L$ (N/mm)	Error (%)
460	469	249	242	2.9
670	994	327	333	1.8
800	1413	384	399	3.7
1000	2208	470	470	0

#### 4. Concluding comment

In this paper, an experimental device using an infrared camera that enables estimation thermal effects accompanying fretting loading on steel in a cylinder on flat contact configuration was presented. Thermal measurement was coupled to a markers tracking method to eliminate rigid body movements induced by vibrations and rigidity of the fretting device.

During a fretting test with constant loading, results show that the temperature evolution on a pixel and averaged over a zone of interest can be decomposed on a global warming and a sum of two periodic signals at  $f_L$  and  $2f_L$ , where  $f_L$  is the loading frequency. A local least-square fitting was proposed to approximate the temperature evolution. Results show that global warming reaches a stabilized value after several cycles while amplitudes of periodic signals remains constants.

During a fretting test with constant normal force but step by step increasing tangential force, results show that stabilized value of variation of temperature averaged over a ZOI can be empirically connected with crack threshold determined by destructive method. Differences between thermal method and destructive method on the crack thresholds were less than 4%. These differences are very lower than it was expected, so these preliminary results must, as usual, be considered with precaution. Complementary checks and tests should be performed in the near future. Nevertheless, the promising results obtained with thermal measurements are already very encouraging.

In this study, tools for a local study of the temperature field, heat sources determination and new information for plastic modeling were developed.

#### REFERENCES

- [1] Hoepfner DW, Chandrasekaran V, Elliot CB, editors. Fretting fatigue: current technology and practices; ASTM STP 1367, American Society for Testing and Materials, 2000, ISBN 0-8031-2851-7.
- [2] Waterhouse RB. Fretting fatigue. Applied Science publishers; 1981.
- [3] Vincent L, Berthier Y, Godet M. Testing methods in fretting fatigue: a critical appraisal. ASTM STP 1992;1159:33-48.
- [4] Fouvry S, Liskiewicz T, Kapsa Ph, Hannel S, Sauger E. An energy description of wear mechanisms and its applications to oscillating sliding contacts. Wear 2003;255:287-98.
- [5] H. Proudhon, S. Fouvry, and G.R. Yantio "Determination and prediction of the fretting crack initiation: introduction of the (P, Q, N) representation and definition of a variable process volume", International Journal of Fatigue, Volume 28, Issue 7, 2006, Pages 707-713.

- [6] S. Fouvry, Ph. Kapsa, L. Vincent, K. Dang Van, Theoretical analysis of fatigue cracking under dry friction for fretting loading conditions, *Wear* 1996; 195: 21-34
- [7] J.A. Araujo, D. Nowell, Analysis of pad size effects in fretting fatigue using short crack arrest methodologies, *International Journal of Fatigue* 21 (1999) 947–956.
- [8] J.A. Araujo, D. Nowell, Analysis of pad size effects in fretting fatigue using short crack arrest methodologies, *International Journal of Fatigue* 21 (1999) 947–956.
- [9] Galtier A., (1993) Contribution à l'étude de l'endommagement des aciers sous sollicitations uni ou multiaxiale, ENSAM Thesis
- [10] Luong M. P., (1998) Fatigue limit evaluation of metals using an infrared thermographic technique, *Mechanics of Materials*, 28:155-163.
- [11] La Rosa G., Risitano A., (2002) Thermographic methodology for rapid determination of the fatigue limit of materials and mechanical components, *International Journal of Fatigue*, 22, 1, 65-73.
- [12] Liaw Y. B., Wang P. K., Jiang L., Huang J. Y., Kuo R. C. and Huang J. C., (2001), Thermographic investigation of the fatigue behaviour of reactor pressure vessel steels, *Materials Science and Engineering A*, 314:131-139.
- [13] Krapez J.C., Pacou D. and Gardette G., (2000), Lock-in thermography and fatigue limit of metals, *Proceedings of QIRT'2000*, Reims, pp. 277-282.
- [14] C. Doudard, M. Poncelet, S. Calloch, C. Boue, F. Hild, A. Galtier, Determination of an HCF criterion by thermal measurements under biaxial cyclic loading, *International Journal of Fatigue* 29 (2007) 748–757
- [15] P. Cugy, Galtier A., (2002), Microplasticity and temperature increase in low carbon steels, *Proceedings 8<sup>th</sup> Int. Fatigue Conference*, Stockholm, pp. 549-556.
- [16] B. Berthel, B. Wattrisse, A. Chrysochoos et A. Galtier (2007) « Thermographic analysis of fatigue dissipation properties of steel sheets », *Strain – An international Journal for Experimental Mechanics*, 43, 3, p273-279. doi: 10.1111/j.1475-1305.2007.00349.x
- [17] Fouvry S., Kapsa P., Vincent L., A multiaxial fatigue analysis of fretting contact taking into account the size effect. *Fretting fatigue: current technology and practices*, ASTM STP 1367; 2000. p. 167-83.
- [18] Fouvry S., Kapsa P., Vincent L., Quantification of fretting damage *Wear*, 1996; 200: 186-205.
- [19] Proudhon H., Fouvry S., Buffière J.-Y., A fretting crack initiation prediction taking into account the surface roughness and the crack nucleation process volume. *International Journal of Fatigue*, 2005. 27: p. 569-579.
- [20] Boulanger T., Chrysochoos A., Mabru C., Galtier A., (2004), Calorimetric and thermoelastic effects associated with the fatigue behavior of steels, *Int. J. of Fatigue*, 26:221-229